ELSEVIER

Journal of Fluids and Structures 22 (2006) 229–252

JOURNAL OF FLUIDS AND STRUCTURES

www.elsevier.com/locate/jfs

A unified approach to aerodynamic damping and drag/lift instabilities, and its application to dry inclined cable galloping

J.H.G. Macdonald[a,*], G.L. Larose[b]

[a]*Department of Civil Engineering, University of Bristol, Queen's Building, University Walk, Bristol BS8 1TR, UK*
[b]*Aerodynamics Laboratory, National Research Council Canada, 1200 Montreal Road, Ottawa, Canada K1A 0R6*

Received 25 August 2004; accepted 16 October 2005

Abstract

Inclined cables of cable-stayed bridges often experience large amplitude vibrations. One of the potential excitation mechanisms is dry inclined cable galloping, which has been observed in wind tunnel tests but which has not previously been fully explained theoretically. In this paper, a general expression is derived for the quasi-steady aerodynamic damping (positive or negative) of a cylinder of arbitrary cross-section yawed/inclined to the flow, for small amplitude vibrations in any plane. The expression covers the special cases of conventional quasi-steady aerodynamic damping, Den Hartog galloping and the drag crisis, as well as dry inclined cable galloping. A nondimensional aerodynamic damping parameter governing this behaviour is proposed, which is a function of only the Reynolds number, the angle between the wind velocity and the cable axis, and the orientation of the vibration plane. Measured static force coefficients from wind tunnel tests have been used with the theoretical expression to predict values of this parameter. Two main areas of instability (i.e. negative aerodynamic damping) have been identified, both in the critical Reynolds number region, one of which was previously observed in separate wind tunnel tests on a dynamic cable model. The minimum values of structural damping required to prevent dry inclined cable galloping are defined, and other factors in the behaviour in practice are discussed.

Keywords: Aerodynamic damping; Den Hartog galloping; Drag crisis; Dry inclined cable galloping; Reynolds number; Quasi-steady theory

1. Introduction

Large amplitude flow-induced vibrations of inclined cables, such as on cable-stayed bridges, are surprisingly common. Various mechanisms could be responsible, including rain-wind excitation, von Kármán vortex shedding, motion of the cable ends, high reduced velocity vortex shedding and dry inclined cable galloping. The very low inherent damping of long cables is also a contributing factor, but it remains uncertain what level of structural damping is required to prevent the vibrations.

Dry inclined cable galloping has only recently been considered as an excitation mechanism. Here the term is taken to refer to divergent self-excited vibrations in the critical Reynolds number range, as have been observed in wind tunnel

*Corresponding author. Tel.: +44 117 928 9758; fax: +44 117 928 7783.
E-mail address: john.macdonald@bristol.ac.uk (J.H.G. Macdonald).

0889-9746/$ - see front matter © 2005 Elsevier Ltd. All rights reserved.
doi:10.1016/j.jfluidstructs.2005.10.002

tests at the National Research Council, Canada (Cheng et al., 2003a). Vibrations of dry inclined or yawed circular cylinders have also been observed in wind tunnel tests elsewhere, notably by Saito et al. (1994), although different excitation mechanisms could be responsible, since these other tests have generally been at lower Reynolds numbers. Other potential mechanisms include high reduced velocity vortex shedding (Matsumoto, 1998), or asymmetric effects of the axial flow and/or cylinder end conditions in the wind tunnel.

On actual cable-stayed bridges, several occurrences of cable vibrations, in the absence of rain, have not been fully explained [see for example Langsoe and Larsen (1987) for the Faro Bridges and Melby et al. (1994) for the Helgeland Bridge]. Although in some cases excitation mechanisms have been suggested, direct evidence has often been lacking since insufficient measurements of the responses and wind and traffic conditions have been available. There is clearly a need for greater understanding of the possible excitation mechanisms, which include dry inclined cable galloping.

Some more detailed records of inclined cable vibration events have recently been reported for the Øresund Bridge (Svensson et al., 2004). The majority of events occurred in freezing conditions and were attributed to galloping-type vibrations associated with ice accretion on the cables. This does seem very likely to have been the case, as for the familiar Den Hartog galloping of iced transmission lines (Den Hartog, 1956). However, a proper analysis would need to consider the three-dimensional geometry for inclined cables. The general method presented here could cover such a situation, if suitable force coefficient measurements were available.

Furthermore, some other cable vibration events on the Øresund Bridge occurred in the absence of ice or rain (Svensson et al., 2004). Although it was suggested these could be due to parametric excitation, there was no direct evidence. An alternative explanation of dry inclined cable galloping, governed by critical Reynolds number (Re) effects, is possible. For the 250 mm diameter cables used, the wind speed corresponding to the critical Re would be approximately 20 m/s, or lower considering wind turbulence and cable surface roughness. The measured wind speeds for the incidences of dry (no ice) vibrations were 12–21 m/s. This agreement of the wind speed may not be coincidental.

It was first pointed out by Larose and Zan (2001) that typical cable-stayed bridge cables in high winds reach the critical Re range, which has a strong influence on the aerodynamic forces they experience, and could lead to aerodynamic instabilities such as dry inclined cable galloping. In particular, for a circular cylinder in the critical Re range, there is a rapid drop in the drag coefficient with increasing Re, and there is also significant lift over a narrow range of Re (Schewe, 1983). These changes in the mean force coefficients are due to reattachment of the turbulent boundary layer and formation of laminar separation bubbles, on each side of the cylinder. Furthermore, for yawed/inclined circular cylinders, although at sub-critical Re only the component of flow normal to the cylinder is important in determining the aerodynamic forces, in the critical and super-critical ranges this no longer holds (ESDU, 1986), so the full three-dimensional geometry should be considered.

For a cylinder free to vibrate, if quasi-steady theory can be taken to apply (discussed in Section 4), the changes in the relative velocity over the vibration cycle cause corresponding changes in the aerodynamic forces. This normally gives positive aerodynamic damping for circular cylinders (Macdonald, 2002), but in the critical Re range the force variations can be adverse, due to the local changes in the force coefficients. This can lead to negative aerodynamic damping, and hence a galloping-type instability. This is very similar to classical Den Hartog galloping (Den Hartog, 1956), for which the changes in the flow regime, giving adverse changes in the lift coefficient, are instead due to variation of the relative direction of the flow.

There has previously been little analysis of Re effects on yawed/inclined cables. This paper aims to provide a framework for their analysis, with particular emphasis on dry inclined cable galloping. Critical Re and/or three-dimensional effects could also be significant in other applications, such as the following:

(i) Guyed masts, for which the geometry is very similar to inclined bridge cables. Guy cables are typically of smaller diameter, but they often have a rougher surface, which reduces the critical Re (ESDU, 1986), so it could still be reached in strong winds.

(ii) Electricity transmission lines. The problem of Den Hartog galloping of iced transmission lines is well known (Den Hartog, 1956). However, recent measurements of galloping on a test line (Van Dyke and Laneville, 2004) indicate that the worst condition is not necessarily for the wind perpendicular to the line, as is normally assumed. Full three-dimensional treatment of the problem is therefore required. Furthermore, occasionally spirally stranded cables are observed to exhibit galloping behaviour in the absence of ice. On the 275 kV Severn Crossing Conductor, the wind conditions for galloping were found to coincide with the critical Re and 10–30° skewed wind directions (relative to normal to the conductor), for which the spiral stranding caused asymmetric boundary layer transitions, generating significant lift (Davis et al., 1963).

(iii) Marine piles and other slender structures in tidal flows, for which the rapid drop in drag coefficient in the critical Re region has been suggested as a possible cause of streamwise oscillations (Martin et al., 1981).

Whilst there is much information in the literature about the flow around a circular cylinder for flow normal to its axis, there are few reported tests for cylinders yawed/inclined relative to the flow, particularly in the critical Re region. A rare exception was a study by Bursnall and Loftin (1951), who measured mean pressure distributions for a series of specific yaw angles and Reynolds numbers. More extensive wind tunnel tests have only recently been conducted on inclined circular cylinders at the National Research Council Canada (NRC), in collaboration with RWDI Inc. and the University of Ottawa. Firstly, a series of tests were conducted on a full-scale cable section elastically supported to simulate the dynamics of an inclined cable (Cheng et al., 2003a). One particular configuration, designated set-up 2C, exhibited divergent amplitude vibrations at a wind speed of 32 m/s. Secondly, detailed pressure measurements were taken on a smaller diameter static circular cylinder, in a different wind tunnel, varying both the inclination and yaw angles in wind velocities spanning the critical Re range (Larose et al., 2003).

It has been suggested that dry inclined cable galloping is caused by a modified Den Hartog galloping instability, with some supporting evidence from the wind tunnel test results (Cheng et al., 2003b), although the theoretical basis for this has been lacking. Recently, in parallel with the current work, Carassale et al. (2004) have considered a three-dimensional quasi-static model of the behaviour, but not including the changes in force coefficients with Re.

The present paper aims to clarify the mechanism of dry inclined cable galloping. Firstly, a general theoretical expression is derived for the quasi-steady aerodynamic damping of vibrations of any yawed/inclined cylinder in any given plane, including 3-D and Re effects. This is shown to cover the special cases of Den Hartog galloping, conventional quasi-steady aerodynamic damping, the drag crisis and sub-critical aerodynamic damping of inclined cables. It is then applied to the case of dry inclined cable galloping, using the measured pressure data from the NRC static model tests in the critical Re region, yielding theoretical values of negative aerodynamic damping that must be overcome by structural damping to prevent the instability from occurring. The analysis successfully predicts the galloping behaviour observed in the NRC dynamic model tests.

2. Derivation of theoretical aerodynamic damping

A general expression for the theoretical aerodynamic damping is derived, based on quasi-steady theory. The resulting aerodynamic damping may be either positive or negative. When negative, it indicates a galloping-type aerodynamic instability, unless counteracted by sufficient structural damping.

A cylinder of arbitrary cross-section is considered, in a flow velocity U at an angle relative to the cylinder axis of ϕ, known here as the cable–wind angle (Fig. 1(a)). If the cylinder moves with velocity v in the plane normal to its axis in a direction at angle α to the cable–wind plane (Figs. 1 and 2), the magnitude of the relative incident velocity is

$$U_R = \sqrt{U^2 - 2Uv \sin\,\phi\,\cos\,\alpha + v^2}. \tag{1}$$

The direction of the projection of the relative velocity in the plane normal to the cylinder axis (U_{NR}), relative to the normal component of the actual flow velocity (U_N) is given by (Fig. 2(b))

$$\tan\,\alpha_D = \frac{v\,\sin\,\alpha}{U\,\sin\,\phi - v\,\cos\,\alpha}. \tag{2}$$

The relative velocity causes drag and lift forces on the cylinder, per unit length, normal to its axis, given by

$$F_D = \tfrac{1}{2}\rho U_R^2 D C_D \quad \text{and} \quad F_L = \tfrac{1}{2}\rho U_R^2 D C_L,$$

where ρ is the fluid density, D is a representative dimension of the cylinder cross-section (taken to be the diameter for a circular cylinder), and C_D and C_L are the drag and lift coefficients, respectively.

It should be noted that D is a dimension of the cross-section itself, independent of the direction of the relative velocity. C_D and C_L are defined with respect to D and U_R, the magnitude of the relative velocity (rather than the component of velocity normal to the cylinder, as sometimes used elsewhere).

The angle between the drag force and the direction of cylinder motion is given by (Fig. 2(b))

$$\alpha_R = \alpha + \alpha_D. \tag{3}$$

Hence, the component of the resultant force, per unit length, acting in the direction of the cylinder velocity, v, is

$$F_v = \tfrac{1}{2}\rho U_R^2 D[C_D\,\cos(\alpha + \alpha_D) - C_L\,\sin(\alpha + \alpha_D)]. \tag{4}$$

This force is a function of the cylinder velocity, v, but not of its displacement or acceleration, since it is based on the quasi-steady approach. It therefore effectively provides a nonlinear damping term in the equation of motion of the

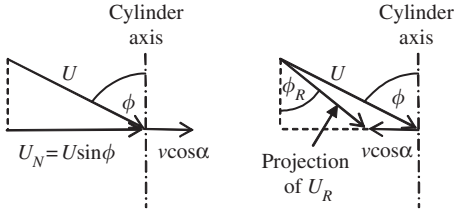

(a) **Absolute velocities** (b) **Velocities relative to cylinder**

Fig. 1. Velocities in the plane of the cylinder axis and the flow velocity vector (also known as the cable–wind plane).

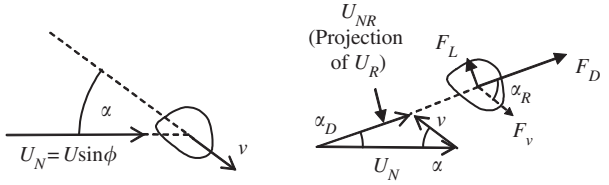

(a) **Absolute velocities** (b) **Velocities relative to cylinder, and resulting forces**

Fig. 2. Velocities and forces in the plane normal to the cylinder axis.

cylinder. For small amplitude vibrations in a given mode (i.e. at the onset of vibrations), the equivalent linear aerodynamic damping ratio is thus given by

$$\zeta_a = \frac{-1}{2m\omega_n}\frac{\mathrm{d}F_v}{\mathrm{d}v}\bigg|_{v=0}, \tag{5}$$

where m is the cylinder mass per unit length and ω_n is the undamped circular natural frequency.

For a uniform cylinder in uniform flow, this expression is independent of the mode shape of vibrations, since the integral functions, involving the mode shape, over the cylinder length for the generalized mass, stiffness and damping force are all identical and therefore cancel out.

Differentiating Eq. (4), substituting into Eq. (5), and noting that when $v = 0$, $U_R = U$ and $\alpha_D = 0$, the following general expression for the small amplitude aerodynamic damping (positive or negative) is obtained:

$$\zeta_a = \frac{-\rho DU}{4m\omega_n}\left\{2\frac{\mathrm{d}U_R}{\mathrm{d}v}(C_D\cos\alpha - C_L\sin\alpha) + U\left[\frac{\mathrm{d}C_D}{\mathrm{d}v}\cos\alpha + C_D\frac{d}{\mathrm{d}v}(\cos(\alpha+\alpha_D)) - \frac{\mathrm{d}C_L}{\mathrm{d}v}\sin\alpha - C_L\frac{d}{\mathrm{d}v}(\sin(\alpha+\alpha_D))\right]\right\}_{v=0}. \tag{6}$$

Taking a quasi-steady approach, the force coefficients are a function of only (i) the Reynolds number based on the relative velocity (Re_R), (ii) the angle between the cylinder axis and the projection of U_R in the cable–wind plane (ϕ_R), and (iii) the angle of attack of the normal component of U_R (U_{NR}) relative to the direction of motion in the plane normal to the cylinder axis (α_R) (Figs. 1 and 2). Hence,

$$\frac{\mathrm{d}C_F}{\mathrm{d}v} = \frac{\partial C_F}{\partial \mathrm{Re}_R}\frac{\mathrm{d}\mathrm{Re}_R}{\mathrm{d}v} + \frac{\partial C_F}{\partial \phi_R}\frac{\mathrm{d}\phi_R}{\mathrm{d}v} + \frac{\partial C_F}{\partial \alpha_R}\frac{\mathrm{d}\alpha_R}{\mathrm{d}v}, \tag{7}$$

where $C_F = C_D$ or C_L, and $\mathrm{Re} = \rho DU/\mu$ is the Reynolds number based on the cylinder cross-sectional dimension and the magnitude of the undisturbed flow velocity (rather than the normal component), and μ is the dynamic (absolute) fluid viscosity.

In Eq. (7), the subscript R refers to relative quantities, allowing for the cylinder velocity. The subscripts may be dropped from the partial derivatives of the force coefficients, based on the quasi-steady approach.

The detailed evaluation of the definite derivatives in Eqs. (6) and (7) is given in Appendix A, finally leading to the general expression for aerodynamic damping for small amplitude vibrations of a cylinder in any given plane:

$$\zeta_a = \frac{\mu \mathrm{Re}}{4m\omega_n}\cos\alpha\left\{\cos\alpha\left[C_D\left(2\sin\phi+\frac{\tan^2\alpha}{\sin\phi}\right)+\frac{\partial C_D}{\partial \mathrm{Re}}\mathrm{Re}\sin\phi+\frac{\partial C_D}{\partial\phi}\cos\phi-\frac{\partial C_D}{\partial\alpha}\frac{\tan\alpha}{\sin\phi}\right]\right.$$
$$\left.-\sin\alpha\left[C_L\left(2\sin\phi-\frac{1}{\sin\phi}\right)+\frac{\partial C_L}{\partial \mathrm{Re}}\mathrm{Re}\sin\phi+\frac{\partial C_L}{\partial\phi}\cos\phi-\frac{\partial C_L}{\partial\alpha}\frac{\tan\alpha}{\sin\phi}\right]\right\}. \quad (8)$$

This expression covers the general case of effects due to any function of the static force coefficients, including conventional quasi-steady aerodynamic damping, Den Hartog galloping, and Re effects such as the drag crisis and dry inclined cable galloping.

3. Special cases of quasi-steady aerodynamic damping and lift/drag instabilities

3.1. Den Hartog galloping

For across-flow vibrations in flow normal to the cylinder axis (i.e. $\phi = 90^\circ$ and $\alpha = 90^\circ$), and noting that $\mu\mathrm{Re} = \rho DU$, Eq. (8) reduces to

$$\zeta_a = \frac{\rho DU}{4m\omega_n}\left(C_D+\frac{\partial C_L}{\partial\alpha}\right). \quad (9)$$

This includes the familiar Den Hartog criterion for galloping occurrence, in the absence of structural damping, if (Den Hartog, 1956)

$$C_D+\frac{\partial C_L}{\partial\alpha}<0.$$

For flow from other directions, but still with $\alpha = 90^\circ$, Eq. (9) can be correctly modified by using the component of flow velocity normal to the cylinder axis, and the force coefficients based on the same component of the flow (although, in general, these modified force coefficients can still potentially be functions of ϕ).

3.2. Drag crisis

Eq. (8) also applies to the potential instability in the direction of the flow, due to the rapid drop of the drag coefficient in the critical Re region, known as the drag crisis or drag instability. In this case, $\phi = 90^\circ$ and $\alpha = 0$, so the expression reduces to

$$\zeta_a = \frac{\mu \mathrm{Re}}{4m\omega_n}\left(2C_D+\frac{\partial C_D}{\partial \mathrm{Re}}\mathrm{Re}\right). \quad (10)$$

Hence the aerodynamic damping becomes negative if

$$2C_D+\frac{\partial C_D}{\partial \mathrm{Re}}\mathrm{Re}<0, \quad (11)$$

which is the drag crisis equivalent of the Den Hartog galloping criterion. This was first proposed by Martin et al. (1981), regarding streamwise oscillations of circular marine piles in tidal flows. This potential instability has also been investigated as a possible cause of along-wind vibrations of lighting columns (Owen, 2002; Smith and Wyatt, 2003).

3.3. Conventional quasi-steady aerodynamic damping

Outside the critical Re region, or for sharp-cornered sections insensitive to Re, such as bluff bridge decks, Eq. (10) reduces further to the more familiar equation for the quasi-steady aerodynamic damping for vibrations in the direction of the flow, as proposed by Davenport (1962):

$$\zeta_a = \frac{\rho DUC_D}{2m\omega_n}. \quad (12)$$

For flow from different directions, but maintaining $\alpha = 0$, this expression can be correctly modified by using the normal component of the flow and the drag coefficient based on this flow component, if this coefficient can be assumed to be invariant with ϕ.

Eq. (9) also covers conventional quasi-steady aerodynamic damping for across-flow vibrations. For wide sections such as typical bridge decks, $\partial C_L/\partial\alpha \gg C_D$, so the aerodynamic damping is reasonably approximated by

$$\zeta_a \approx \frac{\rho D U}{4m\omega_n}\frac{\partial C_L}{\partial\alpha}, \tag{13}$$

as also proposed by Davenport (1962).

For a circular cylinder, $\partial C_L/\partial\alpha = 0$, and Eq. (9) for the across-flow aerodynamic damping in flow normal to the cylinder axis reduces to

$$\zeta_a = \frac{\rho D U C_D}{4m\omega_n}, \tag{14}$$

i.e. half of the aerodynamic damping for vibrations in the direction of the flow, in the sub-critical Re range (Eq. (12)), as noted by Virlogeux (1998).

4. Application to inclined circular cylinder

The general expression of Eq. (8) is applicable to a cylinder of any cross-section, if quasi-steady theory can be taken to apply. A special case of particular interest is that of a circular cylinder inclined and yawed relative to the flow, potentially leading to dry inclined cable galloping of bridge stay cables.

In this case the critical Re is approximately 3×10^5, which for typical bridge cable diameters (150–300 mm) corresponds to wind speeds of 15–30 m/s, or lower depending on the wind turbulence and surface roughness (ESDU, 1986). For typical cable frequencies (of the order of 1 Hz), this equates to reduced velocities of the order of 100. Hence it can be argued that it is likely that the steady flow conditions have time to develop throughout the vibration cycle, so the assumption of quasi-steady theory is reasonable.

For a circular cylinder, the force coefficients are invariant with the angle of attack (α), i.e.

$$\frac{\partial C_D}{\partial\alpha} = \frac{\partial C_L}{\partial\alpha} = 0.$$

The section is always symmetrical, but asymmetrical forces can still be developed within the critical Re range, when, with increasing Re, a laminar separation bubble forms on one side of the cylinder before the other (Schewe, 1983). This gives an asymmetric flow, and hence generates a mean lift force over a narrow range of Re. However, the direction of this mean lift force is arbitrary, depending on which side of the symmetrical section the first laminar separation bubble happens to form. Therefore, in the formulation, the terms relating to the lift force may be either positive or negative, which may be either beneficial or detrimental, depending on the directions of the lift force and the cylinder velocity.

The aerodynamic damping of a circular cylinder, in any orientation relative to the flow, is therefore given by

$$\begin{aligned}\zeta_a = \frac{\mu\mathrm{Re}}{4m\omega_n}\cos\alpha\Bigg\{&\cos\alpha\left[C_D\left(2\sin\phi+\frac{\tan^2\alpha}{\sin\phi}\right)+\frac{\partial C_D}{\partial\mathrm{Re}}\mathrm{Re}\sin\phi+\frac{\partial C_D}{\partial\phi}\cos\phi\right]\\ &\pm\sin\alpha\left[C_L\left(2\sin\phi-\frac{1}{\sin\phi}\right)+\frac{\partial C_L}{\partial\mathrm{Re}}\mathrm{Re}\sin\phi+\frac{\partial C_L}{\partial\phi}\cos\phi\right]\Bigg\}.\end{aligned} \tag{15}$$

It is assumed in this analysis that the sign of the lift force, although arbitrary when the asymmetry first occurs, then remains constant. This is based on the fact that the asymmetric flow regime, once initiated, is stable (Schewe, 1983), so for small amplitude vibrations (i.e. small perturbations of the relative velocity), the lift would not be expected to switch in sign. There are therefore two distinct solutions for the small amplitude aerodynamic damping, as given in Eq. (15), depending on the initial sign of the lift.

4.1. Angle relationships

For a cylinder, e.g. a bridge cable, inclined at an angle θ to the horizontal, in a horizontal flow skewed at angle β relative to the horizontal projection of the cylinder (Fig. 3), the cable–wind angle, ϕ, is given by

$$\cos\phi = \cos\beta\cos\theta.$$

The relationships between β and ϕ are plotted for various inclination angles, θ, in Fig. 4.

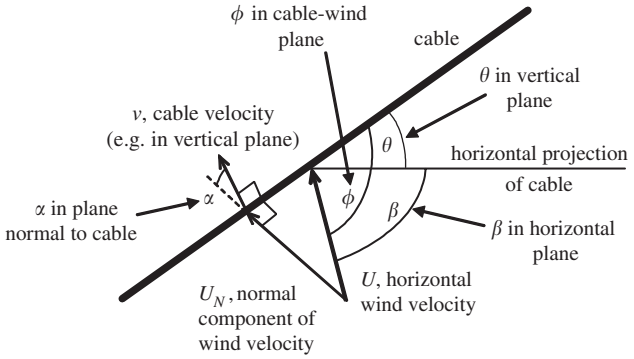

Fig. 3. Geometry of inclined cable in skew wind.

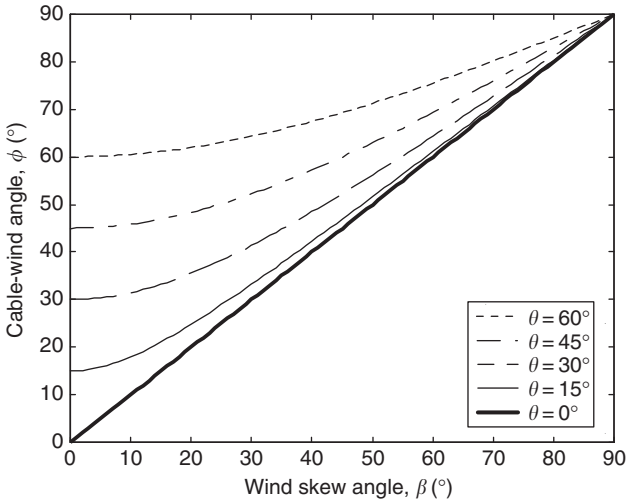

Fig. 4. Relationship between wind skew angle, β, and cable–wind angle, ϕ, for various cable inclination angles, θ.

For vibrations in the vertical plane of the cable, the angle between the cable–wind plane and the plane of motion, α_{IP}, is given by

$$\tan \alpha_{IP} = \frac{\tan \beta}{\sin \theta}, \quad \text{i.e.} \quad \cos \alpha_{IP} = \frac{\tan \theta}{\tan \phi},$$

and for out-of-plane vibrations, the angle between the planes, α_{OP}, is given by

$$\tan \alpha_{OP} = \frac{\sin \theta}{\tan \beta}, \quad \text{i.e.} \quad \sin \alpha_{OP} = \frac{\tan \theta}{\tan \phi}.$$

The relationships of α_{IP} and α_{OP} to β are plotted for various inclination angles, θ, in Fig. 5.

4.2. Aerodynamic damping in sub-critical Re range

In the sub-critical Re range, the lift coefficient is zero and the drag coefficient with respect to the normal component of flow velocity (C_{DN}) may be taken to be constant (ESDU, 1986). Hence

$$C_D = C_{DN} \sin^2 \phi, \tag{16a}$$

$$\frac{\partial C_D}{\partial \phi} = 2C_{DN} \sin \phi \cos \phi \quad \text{and} \quad \frac{\partial C_D}{\partial \mathrm{Re}} = C_L = \frac{\partial C_L}{\partial \mathrm{Re}} = \frac{\partial C_L}{\partial \phi} = 0. \tag{16b}$$

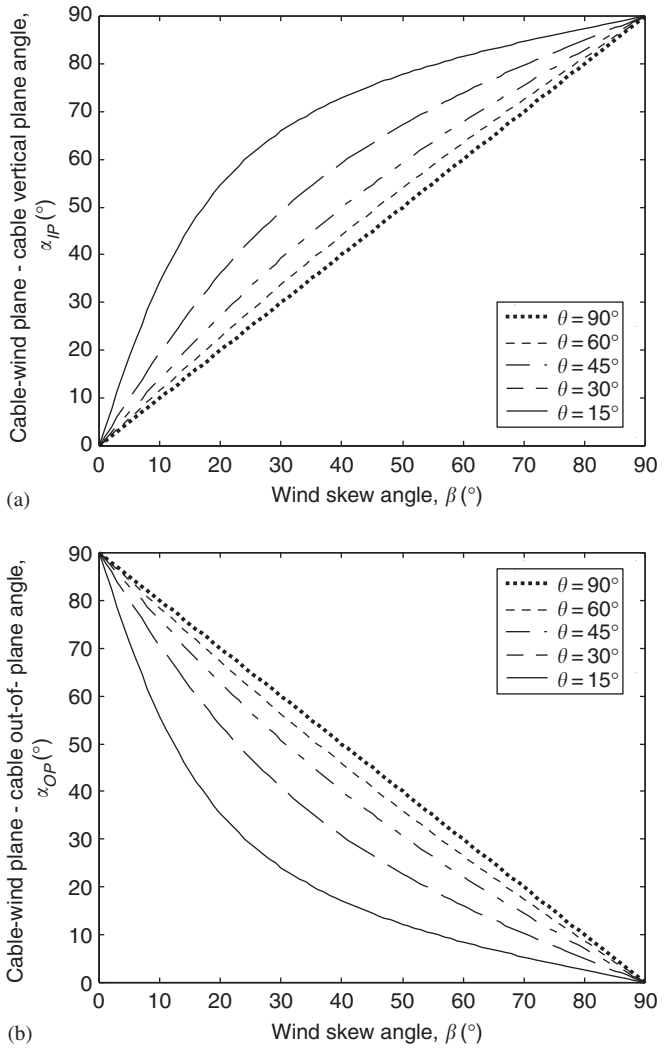

Fig. 5. Relationship between wind skew angle, β, and cable–wind plane—cable vibration plane angle, for various cable inclination angles, θ: (a) in-plane cable motion; (b) out-of-plane cable motion.

Substituting these into Eq. (15), it reduces to

$$\zeta_a = \frac{\rho D U}{4 m \omega_n} C_{DN} \sin \phi (1 + \cos^2 \alpha), \tag{17}$$

which is identical to an expression previously derived for the sub-critical case (Macdonald, 2002). For vibrations in the vertical plane of an inclined cable in a skew flow, this transforms to

$$\zeta_a = \frac{\rho D U}{4 m \omega_n} C_{DN} \sqrt{1 - \cos^2 \theta \cos^2 \beta} \left[1 + \frac{\sin^2 \theta \cos^2 \beta}{(1 - \cos^2 \theta \cos^2 \beta)} \right], \tag{18}$$

again as previously derived,[1] and which was validated against full-scale measurements on a cable-stayed bridge (Macdonald, 2002).

[1] Although note different nomenclature was used.

5. Dry inclined cable galloping

In the critical Re region for yawed/inclined cables, the conditions of zero lift and constant C_{DN} no longer apply. Measured values of the force coefficients are required in this region to determine the aerodynamic damping. If it were negative and greater in magnitude than the structural damping, divergent amplitude vibrations would be initiated. Hence, the maximum magnitude of negative aerodynamic damping from Eq. (15) gives the minimum structural damping required to prevent dry inclined cable galloping.

5.1. Measured mean force coefficients

Wind tunnel measurements were conducted on the static pressure tap model in a range of wind speeds and yaw angles for two different inclination angles (Larose et al., 2003). The mean drag and lift coefficients for each test were averaged over four rings of pressure taps (excluding one additional ring too close to the cylinder end), to reduce effects of any axial structure of the flow around the cylinder, to obtain the overall mean force coefficients. The results for the 60° inclined cable are shown in Figs. 6 and 7. The gridlines on Re and cable–wind angle axes show projections of the mesh of measured points. Note that the values of the force coefficients are symmetrical about $\phi = 90°$, as expected for a uniform cylinder.

The mean drag coefficient (Fig. 6) shows the reduction with increasing Re, characteristic of the critical Re region. At sub-critical Re, it also shows the attenuation with cable–wind angle in agreement with Eq. (16), but at super-critical Re there is less attenuation, in accordance with ESDU (1986). The mean lift coefficient (Fig. 7) is close to zero in the sub-critical Re range, but in the critical range ($\mathrm{Re} \approx 3 \times 10^5$) it has large magnitudes, particularly for ϕ close to 90°, due to the single laminar separation bubble. There is also significant variation of the lift coefficient around $\phi \approx 60°$ in the critical Re region. At the highest Re tested ($\mathrm{Re} \approx 3.8 \times 10^5$), the mean lift coefficient is again close to zero for all cable–wind angles, characteristic of super-critical flow with two symmetric laminar separation bubbles.

Measurements on the cylinder inclined at 54.7° yielded very similar results for C_D and C_L, when expressed in terms of the cable–wind angle (ϕ), confirming that this is the significant geometric parameter. For further analysis, the results from the two inclination angles were interpolated at common values of Re and ϕ, and then averaged to find the best estimate of the mean force coefficients.

For a circular cylinder, the sign of the lift coefficient is arbitrary. In practice, in the static cylinder tests, the mean lift was almost always in one direction. This was presumably due to slight asymmetry of the model set-up, e.g. the end conditions, causing the first laminar separation bubble to be tripped preferentially on one side. Once tripped, the asymmetrical flow is stable (Schewe, 1983), so the reversed lift rarely occurred on this model. However, the alternative sign of the lift coefficient has been considered in the analysis (Section 5.4).

5.2. Nondimensional damping parameter

Considering Eq. (15), the only dependence of the aerodynamic damping on the flow velocity and cable diameter is through the Reynolds number. It is also independent of the cable length and the mode shape and number, except as they affect the natural frequency. Also, the cable mass per unit length and natural frequency appear only in the denominator of the first factor. A nondimensional aerodynamic damping parameter is therefore proposed as

$$Z_a = \frac{\zeta_a m f_n}{\mu}, \tag{19}$$

where $f_n = \omega_n/2\pi$ is the natural frequency.

Z_a is then a function only of the Reynolds number and the angles ϕ and α. The equivalent nondimensional structural damping parameter, Z_s, is related to the more familiar nondimensional groups by the relationship

$$Z_s = \frac{\zeta_s m f_n}{\mu} = \mathrm{Sc}\frac{\mathrm{Re}}{U_r}, \tag{20}$$

where ζ_s is the structural damping ratio, $\mathrm{Sc} = m\zeta_s/\rho D^2$ is the Scruton number and $U_r = U/f_n D$ is the reduced velocity. It is suggested that Z_s is a more suitable nondimensional group for Re effects than the Scruton number, which is applicable to reduced velocity effects, such as vortex shedding.

For vibrations in a given mode, the condition for instability to occur is simply

$$Z_a + Z_s < 0. \tag{21}$$

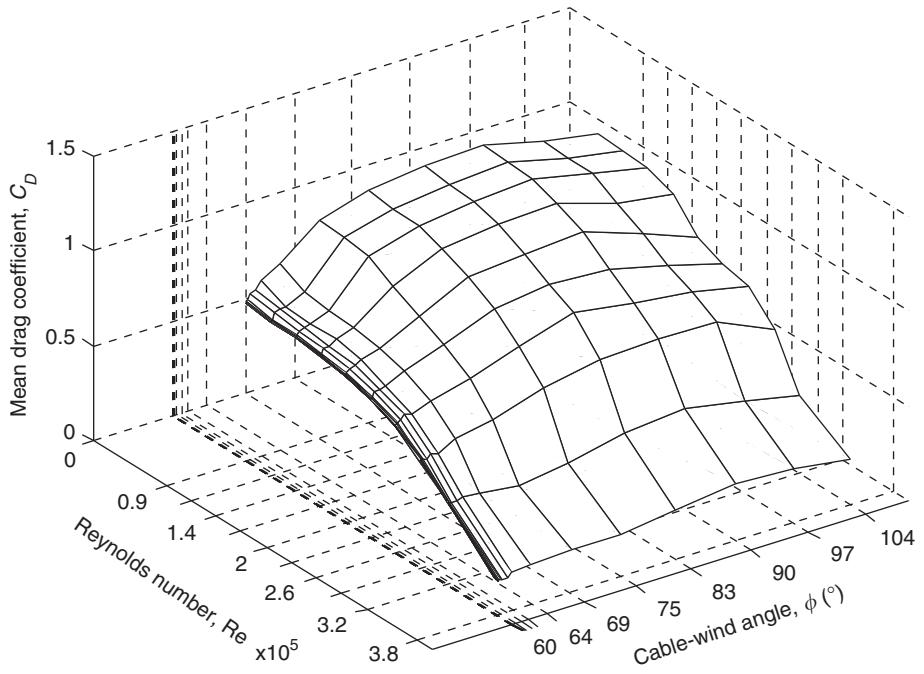

Fig. 6. Mean drag coefficient from wind tunnel tests on 60° inclined cylinder.

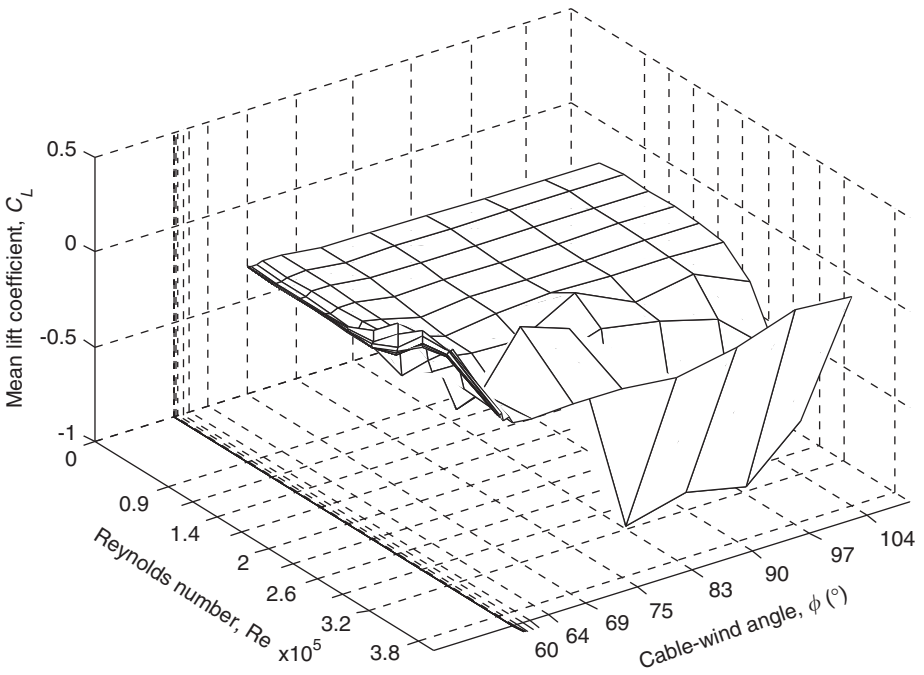

Fig. 7. Mean lift coefficient from wind tunnel tests on 60° inclined cylinder

5.3. Calculated aerodynamic damping values

Taking the measured mean force coefficients and their derivatives from the static model tests (Section 5.1) along with Eqs. (15) and (19), values of the aerodynamic damping parameter can be calculated as a function of Re and cable–wind

angle (ϕ), for any given vibration plane angle (α). The calculated values of Z_a are shown for selected values of α in Figs. 8–13. In these figures, solid contours of Z_a are shown at intervals of 10^4, dotted contours at intervals of 10^3, and a bold contour at $Z_a = 0$, indicating the aerodynamic stability boundary. Darker shading indicates lower (or more negative) values. To relate the values of the nondimensional parameters to a typical bridge cable in air, the values for the dynamic cable tests (Cheng et al., 2003a) are used as an example. For the cable diameter of 160 mm, $\mathrm{Re} = 3 \times 10^5$ corresponds to a wind speed of 28 m/s, and for the cable mass per unit length of 60.8 kg/m and natural frequency 1.4 Hz, $Z_a = 1.0 \times 10^4$ corresponds to an aerodynamic damping ratio of 0.22%.

For across-wind vibrations ($\alpha = 90^\circ$, Fig. 8), for $\mathrm{Re} < 2 \times 10^5$, the aerodynamic damping can be seen to be approximately proportional to Re, in accordance with the sub-critical case discussed in Section 4.2. At higher Re, the aerodynamic damping drops, as the drag coefficient decreases, but it always remains positive so there is no instability. Perhaps surprisingly, there is no influence of the lift coefficient on the small amplitude aerodynamic damping of the across-wind vibrations. This is because, for a circular cylinder, $\partial C_L/\partial\alpha = 0$, due to the rotational symmetry, and the effect of the other lift coefficient terms is dependent on a change in the relative Reynolds number (Re_R), but this change is zero (to first order of v) for across-wind vibrations.

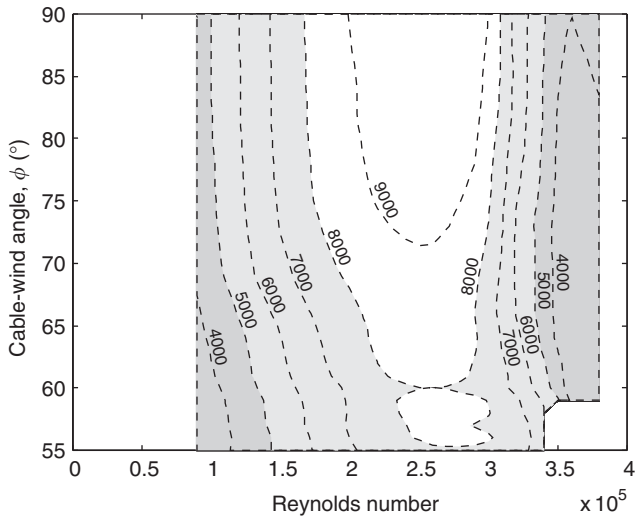

Fig. 8. Aerodynamic damping parameter, Z_a, for $\alpha = 90^\circ$.

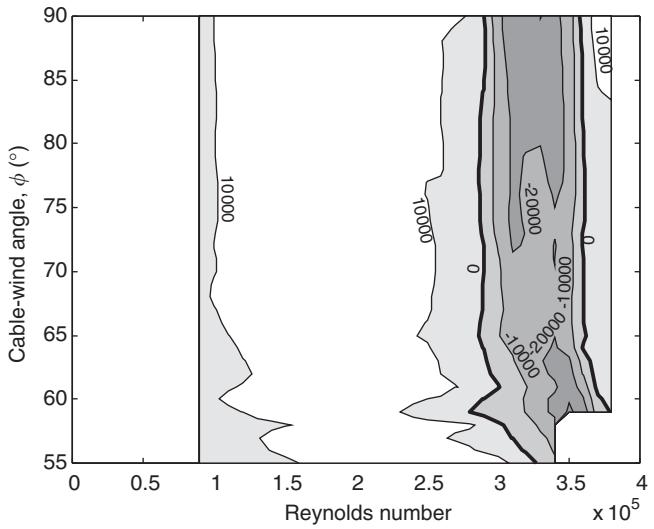

Fig. 9. Aerodynamic damping parameter, Z_a, for $\alpha = 0^\circ$.

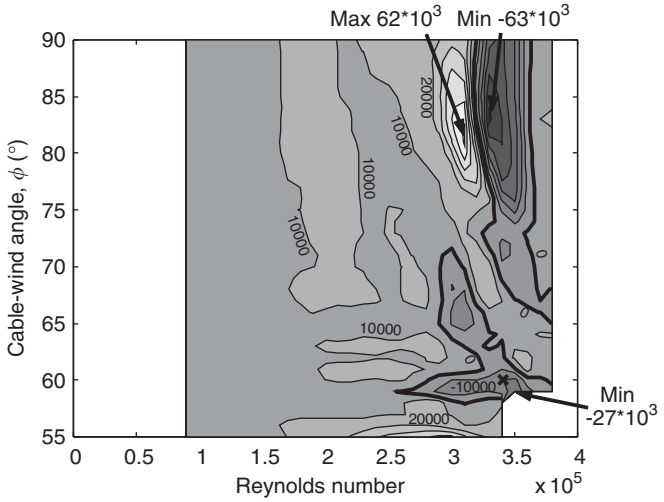

Fig. 10. Aerodynamic damping parameter, Z_a, for $\alpha = 54.7^\circ$. Cross indicates dynamic model test exhibiting large amplitude vibrations.

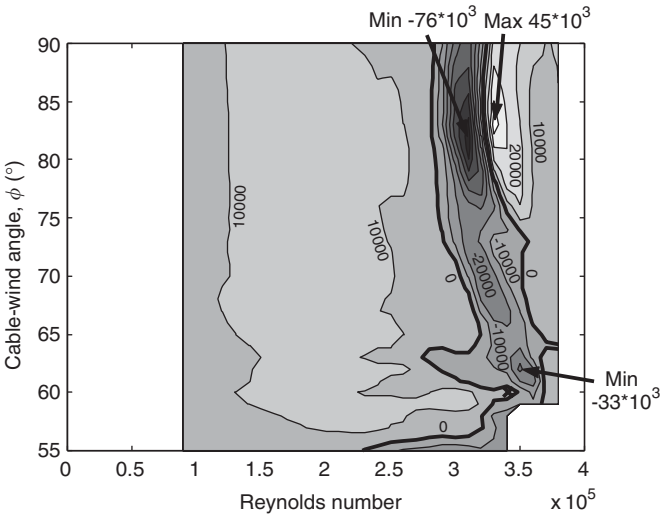

Fig. 11. Aerodynamic damping parameter, Z_a, for $\alpha = -35.3^\circ$.

For along-wind vibrations ($\alpha = 0$, Fig. 9), at low Re, the aerodynamic damping is again positive and approximately proportional to Re, but there is an area of instability for $3.0 \times 10^5 < \mathrm{Re} < 3.6 \times 10^5$, related to the reduction in drag coefficient with Re, i.e. the drag crisis. At higher Re, the cable is again stable.

A particular case of interest is $\alpha = 54.7^\circ$, which corresponds to the test of the dynamic cable model that exhibited divergent amplitude vibrations [set-up 2C, Cheng et al. (2003a)]. The calculated values of the aerodynamic damping parameter, based on the static model test data, are shown in Fig. 10. In this case, the lift coefficient has a significant effect, in contrast to the pure across-wind and along-wind cases (Figs. 8 and 9). This is because the along-wind component of motion (i.e. varying Re_R) generates a change in the lift force, which acts in the direction of the across-wind component of motion, thus providing an effective damping force (positive or negative). The cross in Fig. 10 (and also in Figs. 11–13) indicates the values of Re (3.4×10^5) and ϕ (60°) for which the large amplitude vibrations of the dynamic cable model occurred. It is clear that this was in the centre of a predicted instability region, with $Z_a = -20 \times 10^3$ (i.e. $\zeta_a = -0.44\%$), which supports the proposition that the analysis and the underlying quasi-steady assumption are valid for this situation.

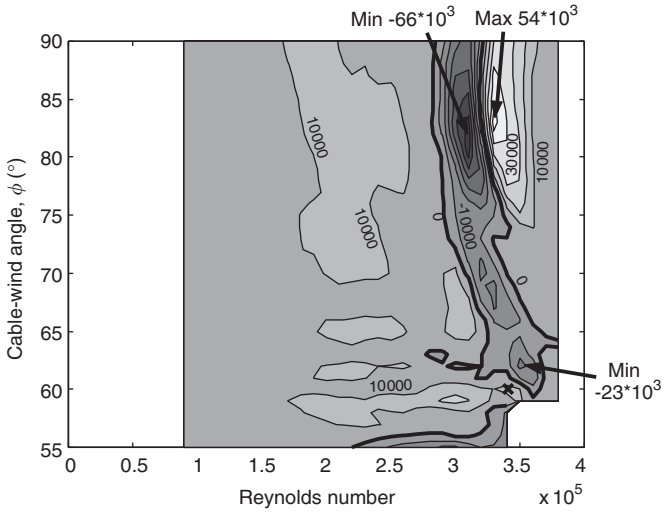

Fig. 12. Aerodynamic damping parameter, Z_a, for $\alpha = -54.7^\circ$.

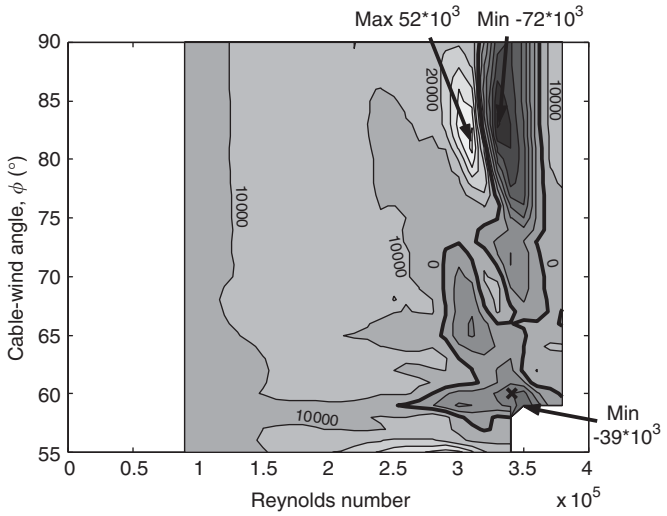

Fig. 13. Aerodynamic damping parameter, Z_a, for $\alpha = 35.3^\circ$.

Fig. 11 shows the calculated aerodynamic damping for vibrations of the dynamic cable model (set-up 2C) in the orthogonal plane ($\alpha = -35.3^\circ$). The cross is then close to an instability boundary, and indeed in the dynamic test there was a small component of motion in this plane also.

5.4. Alternative solutions for reversed sign of lift coefficient

As discussed in Section 4 and shown in Eq. (15), the sign of the lift force on a circular cylinder is arbitrary. There is therefore a second solution for the predicted aerodynamic damping for each vibration plane, with the lift force reversed in sign. This is equivalent to reversing the sign of the vibration plane angle, α. Figs. 12 and 13 therefore show the calculated aerodynamic damping parameter for the alternative solutions for the dynamic model set-up 2C, i.e.

$\alpha = -54.7^\circ$ and 35.3°. This shows that had the first laminar separation bubble, by chance, formed on the other side of the cable, the vibrations in the $(-)54.7^\circ$ plane would have been stable, but instead vibrations in the orthogonal $(+)35.3^\circ$ plane would have been unstable. The results for $\alpha = 54.7^\circ$ and 35.3° (Figs. 10 and 13; and also for $\alpha = -35.3^\circ$ and -54.7°, Figs. 11 and 12) are similar to each other for the whole ranges of Re and ϕ. This because the angles are symmetrical about $\alpha = 45^\circ$ (or -45°), which gives the same product $\cos\alpha \sin\alpha$ applied to the lift coefficient terms in Eq. (15) i.e. the overall damping effect of the lift coefficient is the same, due to the combination of the component of motion along-wind (generating the change in force) and across-wind (on which the force acts to provide damping). Hence the only differences between Figs. 10 and 13 (and Figs. 11 and 12) are due to the contribution of the drag coefficient, which is relatively less important than the lift coefficient (Section 5.6).

5.5. Direct comparison with dynamic cable tests

The dynamic cable tests (Cheng et al., 2003a) were only performed at the specific cable–wind angles $\phi = 35^\circ$, 45° and 60°, whereas the static cylinder pressure measurement tests (Larose et al., 2003) covered cable–wind angles $\phi \geqslant 54.7^\circ$. Hence direct comparisons could only be made for $\phi = 60^\circ$. For this cable–wind angle, only two orientations of the spring supports were considered in the dynamic cable tests, representing $\alpha = 0^\circ$ (and 90°) and 54.7° (and -35.3°). It is important to note that the static and dynamic tests were performed independently, using different wind tunnels, models, cable geometry and end conditions.

Fig. 14 clarifies the theoretical aerodynamic damping for the dynamic test set-up 2C ($\phi = 60^\circ$, $\alpha = 54.7^\circ$) for varying wind speed. It is equivalent to sections through Figs. 10–13 for $\phi = 60^\circ$, with Re and aerodynamic damping parameter converted to wind speed and damping ratio, respectively, for the specific dynamic cable tested. The bold lines correspond to the sign of the lift force as measured in the static wind tunnel tests, while the thinner lines are for the sign of the lift force reversed (expressed as the sign of α reversed). It is clear that at low wind speeds the aerodynamic damping for vibrations in both orthogonal planes ($\alpha = \pm 54.7^\circ$ and 35.3°) is positive (and approximately proportional to wind speed), and indeed in the dynamic tests no significant vibrations were observed. The sign of the lift force has negligible effect in this range, since the flow is virtually symmetrical.

Above ~25 m/s, corresponding to the start of the critical Re range, there are significant changes to the aerodynamic damping. For $\alpha = 54.7^\circ$, and for 35.3° (i.e. in the orthogonal plane, with the lift sign reversed), it becomes negative, indicating instability. Which of these two solutions actually occurs is arbitrary, depending on which side of the cylinder the first laminar separation bubble happens to form, due to perturbations of the flow or slight asymmetry of the cylinder or the wind tunnel set-up. The negative aerodynamic damping values are similar since they are dominated by the magnitude of the lift coefficient, the effect of the drag causing the slight difference (Sections 5.4 and 5.6).

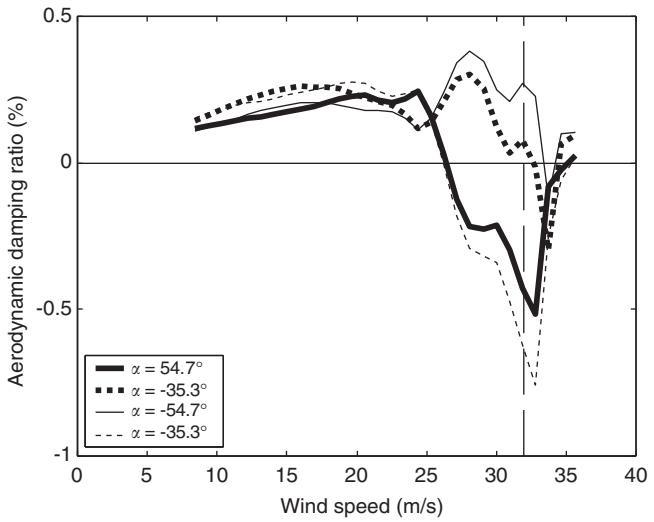

Fig. 14. Theoretical aerodynamic damping ratios of dynamic cable model for $\phi = 60^\circ$. Vertical dashed line indicates wind speed at which dynamic model exhibited large amplitude vibrations for $\alpha = 54.7^\circ$.

In the dynamic model tests, the instability actually occurred in the $\alpha = 54.7^\circ$ plane at a wind speed of 32 m/s, at which the negative aerodynamic damping was sufficient to overcome the structural damping. The theoretical aerodynamic damping for these values was −0.44%. However, the actual structural damping of the dynamic model, for low amplitude vibrations, was only approximately 0.03% (Cheng et al., 2003a). According to Fig. 14, this would suggest that divergent amplitude vibrations should have been expected to start at the lower wind speed of 27 m/s. The slight discrepancy in the onset wind speed is thought to be due to slight differences between the set-ups in the two different wind tunnels, such as cylinder surface roughness and wind turbulence, which affect the critical Re (ESDU, 1986), cable end conditions, or the exact cable–wind angle (ϕ), to which the results are sensitive in the vicinity of $\phi = 60^\circ$ (see Figs. 10–13). Unfortunately, the wind speed was not increased further in the dynamic wind tunnel tests (Cheng et al., 2003a), so it has not been possible to confirm that the cable is again stable in the super-critical region (above approximately 35 m/s), as predicted by the analysis (Fig. 14).

The only other dynamic cable set-up that can be compared directly with theoretical aerodynamic damping values from the static model tests is set-up 2A ($\phi = 60^\circ$, $\alpha = 0^\circ$). In this case no significant along-wind vibrations were observed (Cheng et al., 2003a), although Fig. 9 shows that the drag crisis instability was expected occur for $\mathrm{Re} = 2.9 \times 10^5$ to 3.7×10^5 (i.e. wind speed = 27–35 m/s). The reasons for this discrepancy are not clear, although factors which could be significant include the higher wind turbulence in the dynamic cable tests, and hysteresis of the flow transitions. These and other factors in the general behaviour are discussed further in Section 6.1.

Fig. 8 shows that, according to this analysis, across-wind vibrations ($\alpha = 90^\circ$) are not expected to exhibit instability. In dynamic set-up 2A, indeed no divergent amplitude vibrations were observed, but limited amplitude vibrations did occur in the across-wind direction for wind speeds of 17–19 m/s ($\mathrm{Re} = 1.8 \times 10^5 - 2.0 \times 10^5$, maximum amplitude 67 mm = 0.42D) and at 34 m/s ($\mathrm{Re} = 3.6 \times 10^5$, amplitude 16 mm = 0.10$D$) (Cheng et al., 2003a). With a rougher surface to the cable, across-wind vibrations occurred in wind speeds above 27 m/s ($\mathrm{Re} = 2.9 \times 10^5$), up to the maximum speed tested (38 m/s, $\mathrm{Re} = 4.1 \times 10^5$), with the maximum response of 49 mm (= 0.31D) occurring for 32 m/s ($\mathrm{Re} = 3.4 \times 10^5$). (The rougher cable was not tested for $\alpha = 54.7^\circ$.) Although these wind speeds (for both the smooth and rough cables) are in the general vicinity of the critical Re range, these across-wind vibrations are not predicted by the current analysis. It is likely that they were due to some other mechanism, possibly high reduced velocity vortex shedding (Matsumoto, 1998).

5.6. Areas of instabilities and governing factors

It is notable in Figs. 10–13 (i.e. for $\alpha = \pm 54.7^\circ$ or $\pm 35.3^\circ$) that, as well as the instability around $\phi = 60^\circ$ in Fig. 10, which was validated by the dynamic model tests, there is an area of greater instability predicted for $75^\circ < \phi < 90^\circ$. Unfortunately, measurements were not taken on the dynamic model in this range of ϕ to confirm whether this instability actually occurs. However, it is of interest to determine the governing factors that cause the two main areas of instability. In Eq. (15), there are six terms contributing to the total aerodynamic damping, due to the drag and lift coefficients and each of their derivatives with respect to Reynolds number and cable–wind angle. Fig. 15 shows the individual contribution to the total aerodynamic damping of each of these terms, for the case of $\alpha = 54.7^\circ$.

The contribution from the C_D term (Fig. 15(a)) is always positive, i.e. beneficial. It is the dominant term in the sub-critical Re range ($\mathrm{Re} < 2 \times 10^5$), but in the critical Re region it reduces and it is much smaller in magnitude than some of the other terms. The $\partial C_D/\partial \mathrm{Re}$ term (Fig. 15(b)) gives a significant negative contribution in the critical Re range ($2.8 \times 10^5 < \mathrm{Re} < 3.6 \times 10^5$), particularly for values of ϕ towards 90°. This is the effect of the drag crisis (Section 3.2). The $\partial C_D/\partial \phi$ term (Fig. 15(c)) is small for the full range of parameters tested, so it has little effect on the overall behaviour.

The terms relating to the lift coefficient (Fig. 15(d)–(f)) may be reversed in sign, depending on which side of the cable the first laminar separation bubble happens to form. The C_L term (Fig. 15(d)) is always small compared with the other terms, so it is not very significant. The $\partial C_L/\partial \mathrm{Re}$ term (Fig. 15(e)) has large values (positive or negative) in the critical Re region for $75^\circ < \phi < 90^\circ$. This is the dominant term in causing the major instability in this region. It is associated with the asymmetrical pressure distribution due to the single laminar separation bubble over a narrow range of Re. Finally, the $\partial C_L/\partial \phi$ term (Fig. 15f) is generally small, except in narrow regions around $\phi = 60^\circ$ and $\phi = 55^\circ$, where it is dominant. It is this term which is primarily responsible for the instability observed in the dynamic model test for $\phi = 60^\circ$. The change in mean lift coefficient, and to a lesser extent drag coefficient, with cable–wind angle in this region may be associated with a transition from regular shedding of vortices with axes parallel to the cylinder to a stable structure of vortices (symmetric or asymmetric) with axes close to parallel to the flow near the surface of the cylinder for smaller values of ϕ (Thomson and Morrison, 1971; Lowson and Ponton, 1991).

5.7. Minimum aerodynamic damping

It is of interest to determine the minimum value of the aerodynamic damping for any value of the angle α, for designing against the worst case. Considering Eq. (15), the minimum (or maximum) value occurs when

$$\tan 2\alpha = \pm \frac{g(C_L)}{g(C_D)},$$

where

$$g(C_F) = C_F\left(2\sin\phi - \frac{1}{\sin\phi}\right) + \frac{\partial C_F}{\partial \mathrm{Re}}\mathrm{Re}\sin\phi + \frac{\partial C_F}{\partial\phi}\cos\phi.$$

There are four solutions to this expression, representing the maximum and minimum for the cases of positive or negative lift. However, reversing the sign of the lift simply reverses the sign of α at which the maximum and minimum occur, but the extreme values of the aerodynamic damping parameter itself are the same. Fig. 16 hence shows the minimum aerodynamic damping parameter for any vibration plane. In the region of $3\times10^5 < \mathrm{Re} < 3.5\times10^5$ and $75^\circ < \phi < 90^\circ$, negative aerodynamic damping of very large magnitude occurs, with a minimum value of Z_a of

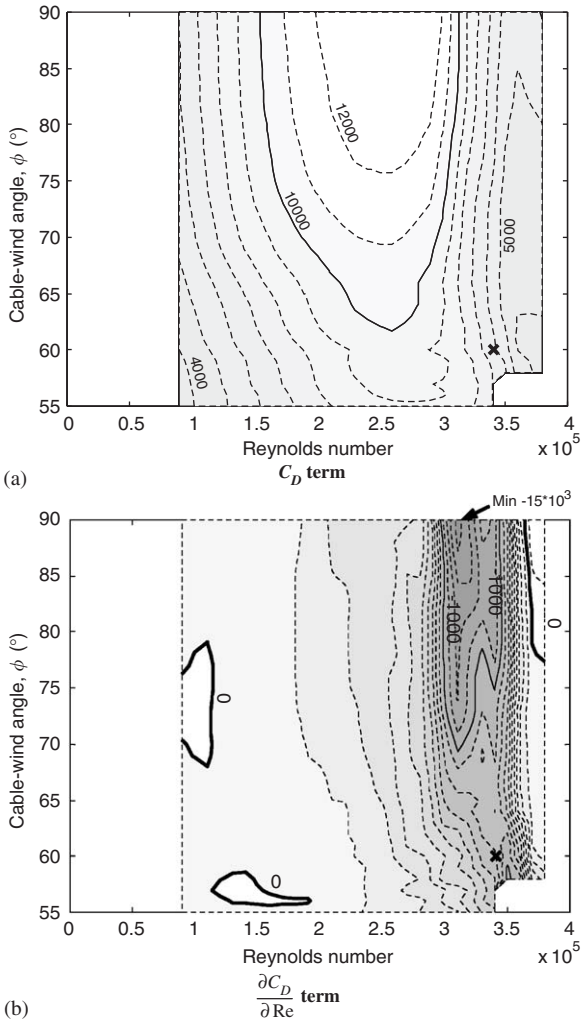

Fig. 15. Contribution to Z_a of each term in Eq. (15), for $\alpha = 54.7^\circ$: (a) C_D term; (b) $\partial C_D/\partial\,\mathrm{Re}$ term; (c) $\partial C_D/\partial\phi$ term; (d) C_L term; (e) $\partial C_L/\partial\mathrm{Re}$ term; (f) $\partial C_L/\partial\phi$ term.

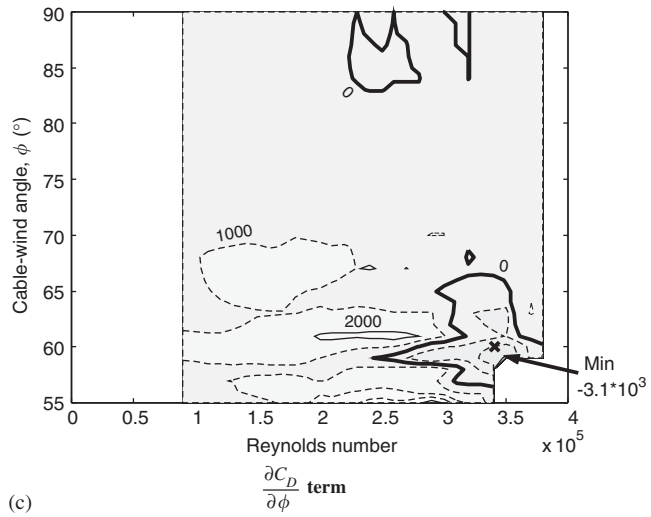

(c)

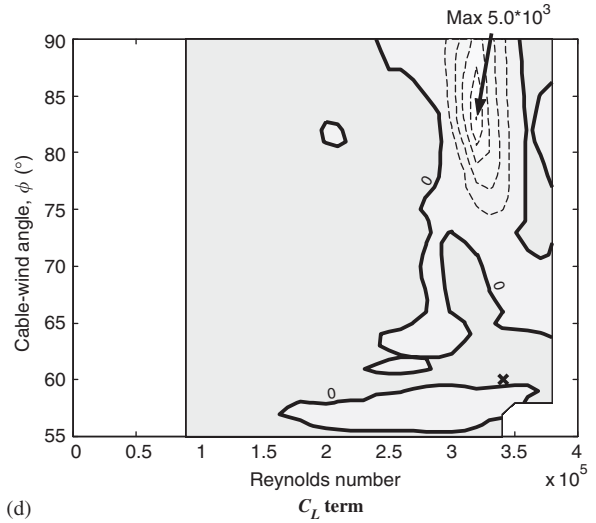

(d)

Fig. 15. (*Continued*)

-76×10^3, giving an aerodynamic damping ratio of -1.7% for the typical cable modelled in the dynamic cable tests (Section 5.3).

Fig. 17 shows the values of the angle α corresponding to the minimum aerodynamic damping values of Fig. 16. In the sub-critical Re range, the angle for the minimum aerodynamic damping (still positive), is generally close to -90°, i.e. with vibrations normal to the cable–wind plane (Section 3.3). However, in the regions of large negative aerodynamic damping, the worst-case angles between the cable–wind and vibration planes are approximately $\pm 30^\circ$.

5.8. Excitation of different modes of vibration and mitigation measures

Although the magnitude of the aerodynamic damping (positive or negative) is inversely proportional to the natural frequency, the aerodynamic stability boundary ($\zeta_a = 0$ in Eq. (8)) is a function only of Re, α and ϕ, and it is independent of the natural frequency, mode number and mode shape. There is therefore potential for a wind velocity in the critical range to excite any mode of the cable. This would actually occur if the negative aerodynamic damping ratio of a given mode were greater in magnitude than its structural damping. The different structural damping of the individual modes is therefore significant for the onset of their vibrations. If the structural damping ratios of different

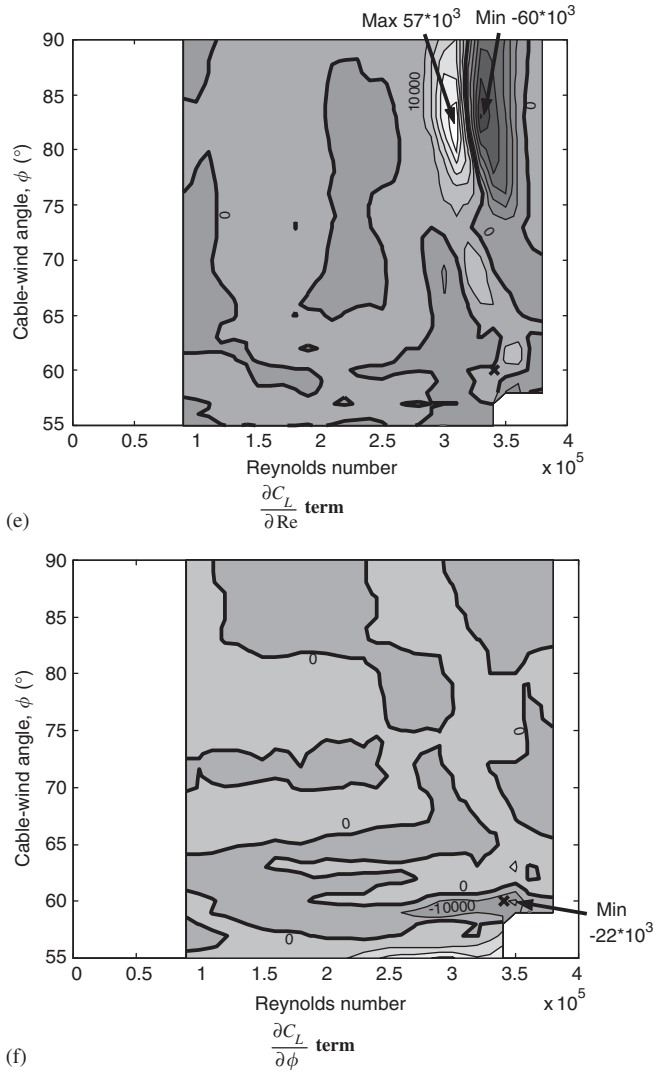

Fig. 15. (*Continued*)

modes were comparable, the lower frequency modes would tend to be excited, since the aerodynamic damping ratio is inversely proportional to natural frequency. In practice, the correlation of the flow velocity over the length of the cable is also likely to be important in determining which modes are excited.

As a Reynolds number effect, the critical wind speed for dry inclined cable galloping is essentially fixed by the cable diameter, which for typical cable stays gives wind speeds of 15–30 m/s. For structural reasons it is not viable to change the diameter sufficiently to avoid the critical Re range. Therefore, the most direct vibration mitigation measures are changing the cross-sectional shape to cause a more gradual transition in the critical Re range, or providing sufficient structural damping to overcome the negative aerodynamic damping. Cable cross-ties have the less direct benefits of increasing the generalized mass of the system and reducing the correlation of the loading over the cable array, as well as possibly increasing the damping of the system.

5.9. Comparison with Den Hartog galloping

A significant difference between dry inclined cable galloping, governed by Eq. (15), and classical Den Hartog galloping (Section 3.1) is that it can occur in only a limited wind speed range, whereas Den Hartog galloping occurs for

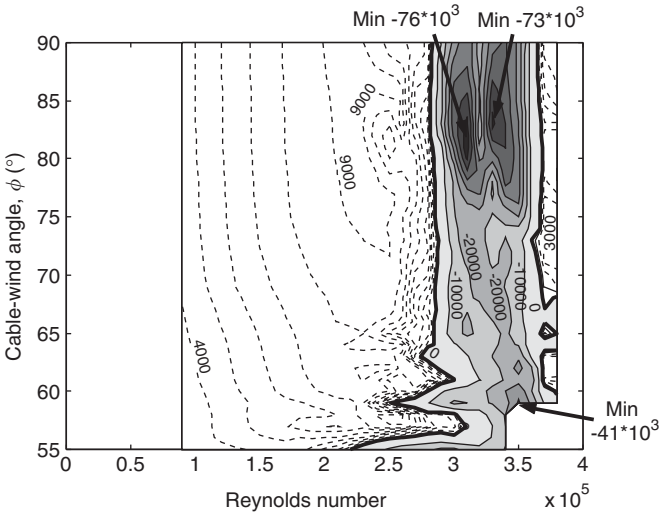

Fig. 16. Minimum aerodynamic damping parameter, Z_a, for any α.

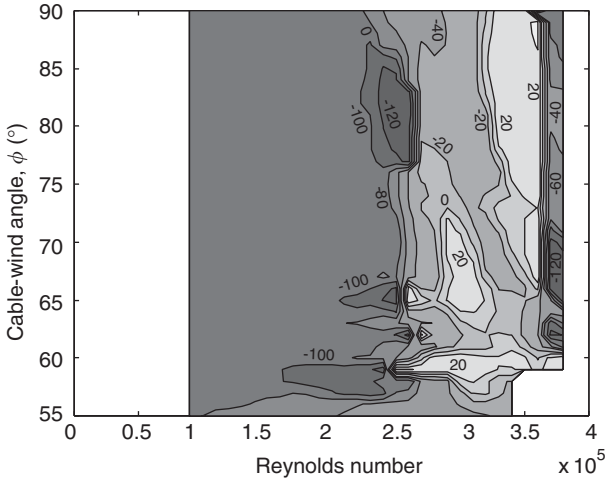

Fig. 17. Value of α (in degrees) corresponding to minimum aerodynamic damping parameter, Z_a, in Fig. 16.

any wind speed above a critical value. Den Hartog galloping is often an issue for bodies with sharp corners, which have force coefficients insensitive to Re. The Den Hartog summation (in brackets in Eq. (9)) therefore has a near-constant value. Galloping occurs if Re is sufficiently large for the negative aerodynamic damping to overcome the structural damping. This occurs when

$$U > \frac{4m\omega_n\zeta_s}{-\rho D\left(C_D + \partial C_L/\partial\alpha\right)}, \tag{22}$$

which may alternatively be expressed in nondimensional form as

$$U_r > \frac{8\pi \mathrm{Sc}}{-\left(C_D + \partial C_L/\partial\alpha\right)} \quad \text{or} \quad \mathrm{Re} > \frac{8\pi Z_s}{-\left(C_D + \partial C_L/\partial\alpha\right)}. \tag{23}$$

In higher wind speeds, the negative aerodynamic damping continues to increase in magnitude and the system becomes even more unstable. In contrast, for dry inclined cable galloping, it has been shown (Section 5.6) that the dominant effects in the behaviour are the changes in force coefficients in the critical Re region. Beyond this region, the force coefficients have near constant values, so the instability no longer exists.

Another characteristic of dry inclined cable galloping is that the vibrations are expected to be limited in amplitude. For large amplitude vibrations, there would be changes in the aerodynamic loads, due to:

(i) variation in the force coefficients and their derivatives over the range of Re and cable–wind angle experienced over the vibration cycle;
(ii) nonlinearity of the damping force of Eq. (4), for $v \neq 0$;
(iii) the breakdown of quasi-steady theory, including (a) changes in the flow structure around the cylinder due to its motion, for example greater correlation along the length of the cylinder, as for vortex lock-in, and (b) the static flow structure not having time to develop due to the changing relative velocity.

Considering the first of these three effects, as the amplitude increases, the relative velocity could go beyond the range for the adverse effect, so the aerodynamic forces may no longer be equivalent to negative damping. In this case, limited amplitude vibrations would be expected, even although the onset was governed by a galloping-type instability. From Figs. 9–13, the instability region covers a Re range, $2\Delta\mathrm{Re}$, of approximately 0.5×10^5. This range would just be spanned by along-wind sinusoidal vibrations with a displacement amplitude equal to

$$A = \frac{\Delta \mathrm{Re}\mu}{\rho D \omega_n}.$$

For the typical cable modelled in the dynamic tests (Section 5.3), this yields a displacement amplitude of 0.27 m ($=1.7D$), although a steady-state would only be reached for a larger amplitude, and for wind other than normal to the cable axis, again the amplitude is likely to be larger.

6. Wider application and additional factors in the behaviour

The above results are for a circular cylinder, representative of most bridge cables. However, some cables have a different profile, some of which have also experienced significant vibrations, which have not been fully explained (Caetano and Cunha, 2003). The excitation mechanism may be similar, and could possibly be described by the general expression of Eq. (8). Furthermore, the results are comparable with site measurements from a cable-stayed bridge in Japan, with longitudinal protrusions on the cables, which experienced significant vibrations in wind speeds of 35–40 m/s in the absence of rain (Matsumoto et al., 1994). At least the first seven modes of vibration were excited, indicating that it was not a frequency-dependent mechanism, such as vortex shedding. The maximum amplitude in the first mode (0.6 Hz) was approximately 0.23 m. The critical conditions, the response in several modes (cf. Section 5.8), and the amplitude of response appear to be reasonably consistent with the analysis of dry inclined cable galloping presented here. However, the evidence is not conclusive and further investigation considering the actual cable profile would be needed to establish the actual excitation mechanism.

It is also likely that the mechanism of rain-wind excitation of inclined cables is related to Re effects (Larose and Zan, 2001), so there could be some similarity with the behaviour considered here. In the presence of rain there are other factors involved, most notably the motion of rivulets on the cable surface, so the mechanism cannot be fully explained by the current analysis. However, the rivulets are likely to affect the separation and reattachment of the boundary layer, thus interacting with and possibly exacerbating the critical Re effects, which could be a significant factor in the instability.

The general method presented could also potentially be used to analyse galloping of iced cables in a 3-D environment (Svensson et al., 2004), or galloping of spirally stranded cables in the absence of ice (Davis et al., 1963), using the appropriate values of the force coefficients.

6.1. Additional factors

For low-frequency cable vibrations, the results above appear to be rather conservative compared with the structural damping ratios of approximately 1% that often seem to be sufficient to mitigate cable vibrations on cable-stayed bridges in practice. Also, although the galloping instability of the dynamic cable model (Cheng et al., 2003b) was

successfully predicted, the analysis suggests that other instabilities should exist, which were not confirmed in the dynamic tests.

Ongoing work is considering the effects of coupling of vibrations in two degrees of freedom, which is potentially beneficial in some circumstances. Also, in practice, the most critical conditions of the two angles, α and ϕ, may not occur simultaneously. Furthermore, the results presented are based on measured force coefficients from the static cable model tests, for which the wind turbulence was low (0.13% longitudinal turbulence intensity) and the model had low surface roughness (effective roughness height $= 7.29 \times 10^{-6} D$). This surface roughness is similar to that of a typical stay-cable HDPE sheath if clean, but accumulated dirt on site may make the roughness greater. Both surface roughness and small-scale turbulence affect the flow transition in the critical Re region (ESDU, 1986). They reduce the critical Re, but also are likely to reduce the severity of the transition, thus reducing the aerodynamic instability. Also, large-scale turbulence would reduce the correlation of the relative wind velocity along the length of the cable.

Another factor that may reduce the severity of the instability in practice is hysteresis of the sharp transitions of the force coefficients in the critical Re region (Schewe, 1983), meaning that small amplitude vibrations may not cause such significant variation in the aerodynamic loads as assumed by the quasi-steady analysis.

7. Conclusions

A general expression has been derived for the quasi-steady aerodynamic damping of a cylinder of arbitrary cross-section yawed/inclined to the flow, for small amplitude vibrations in any plane. The expression covers the general case of effects due to any function of the static force coefficients, including conventional quasi-steady aerodynamic damping, Den Hartog galloping, and Re effects such as the drag crisis and dry inclined cable galloping. Negative aerodynamic damping causes a galloping-type instability, if larger in magnitude than the structural damping.

The expression has been applied to dry inclined cable galloping, which is potentially problematic on cable-stayed bridges. A nondimensional aerodynamic damping parameter has been proposed, which is a function only of Re, the cable–wind angle, ϕ, and the orientation of the vibration plane, α. These have been shown to be the governing parameters for this behaviour, in contrast to the reduced velocity and Scruton number relevant to other excitation mechanisms.

Measured static force coefficients from wind tunnel tests have been used with the theoretical expression to predict the aerodynamic damping values, covering the critical Re range, for cable–wind angles from 54.7° to 90°. Two main areas of instability (i.e. negative aerodynamic damping) have been identified. One occurs in the critical Re region, close to $\phi = 60°$, principally due to the $\partial C_L/\partial\phi$ term. This instability was previously observed in independent wind tunnel tests on a dynamic cable model (Cheng et al., 2003a). The results from the current analysis are in good agreement with the observed behaviour. The second predicted area of instability is more severe and occurs in the critical Re region for $75° < \phi < 90°$. It is principally due to the $\partial C_L/\partial\mathrm{Re}$ term, caused by the existence of high lift from asymmetry of the flow in only a narrow Re range. Unfortunately, the dynamic cable model was not tested in this range of ϕ, so this predicted instability is yet to be validated experimentally. Also an instability was predicted for pure along-wind vibrations, due to the drag crisis (principally from the $\partial C_D/\partial\mathrm{Re}$ term), but this was not apparent in the dynamic cable tests. Further dynamic testing is required to understand the behaviour more fully.

The minimum (i.e. most negative) values of aerodynamic damping predicted define the magnitude of structural damping required to prevent vibrations due to dry inclined cable galloping. However, coupling of two degrees of freedom, wind turbulence, cable surface roughness and hysteresis of the force coefficient transitions may be beneficial and may reduce the level of structural damping required in practice. Further work is required to investigate these effects.

Acknowledgements

This work was conducted during a sabbatical visit of the first author to the National Research Council Canada (NRC) Aerodynamics Laboratory, Ottawa, supported by a Researcher Exchange Award from the joint British Council—NRC Science and Technology Fund.

The wind tunnel tests at NRC were conducted in collaboration with RWDI Inc. and the University of Ottawa, with the financial support of the US Federal Highway Administration and a National Science and Engineering Research Council of Canada grant.

Appendix A

In the main text it was shown that the aerodynamic damping in the general case is given by (Eq. (6))

$$\zeta_a = \frac{-\rho D U}{4 m \omega_n}\left\{2\frac{\mathrm{d}U_R}{\mathrm{d}v}(C_D\cos\alpha - C_L\sin\alpha) + U\left[\frac{\mathrm{d}C_D}{\mathrm{d}v}\cos\alpha + C_D\frac{\mathrm{d}}{\mathrm{d}v}(\cos(\alpha+\alpha_D)) - \frac{\mathrm{d}C_L}{\mathrm{d}v}\sin\alpha - C_L\frac{\mathrm{d}}{\mathrm{d}v}(\sin(\alpha+\alpha_D))\right]\right\}_{v=0}, \tag{A.1}$$

where U_R is the magnitude of the relative incident velocity, given by Eq. (1), from which

$$\left.\frac{\mathrm{d}U_R}{\mathrm{d}v}\right|_{v=0} = -\sin\phi\cos\alpha. \tag{A.2}$$

Also, from the main text (Eq. (7)),

$$\frac{\partial C_F}{\partial v} = \frac{\partial C_F}{\partial \mathrm{Re}_R}\frac{\mathrm{d}\mathrm{Re}_R}{\mathrm{d}v} + \frac{\partial C_F}{\partial \phi_R}\frac{\mathrm{d}\phi_R}{\mathrm{d}v} + \frac{\partial C_F}{\partial \alpha_R}\frac{\mathrm{d}\alpha_R}{\mathrm{d}v}, \tag{A.3}$$

where $C_F = C_D$ or C_L.

The derivatives with respect to v in Eq. (A.3) may be evaluated as follows:

$$\left.\frac{\mathrm{d}\mathrm{Re}_R}{\mathrm{d}v}\right|_{v=0} = \frac{\mathrm{Re}}{U}\left.\frac{\mathrm{d}U_R}{\mathrm{d}v}\right|_{v=0}. \tag{A.4}$$

The angle between the cylinder axis and the projection of U_R in the cable–wind plane (ϕ_R) is given by (Fig. 1(b))

$$\tan\phi_R = \frac{U\sin\phi - v\cos\alpha}{U\cos\phi}. \tag{A.5}$$

Differentiating both sides of Eq. (A.5) with respect to v yields

$$\frac{1}{\cos^2\phi_R}\frac{\mathrm{d}\phi_R}{\mathrm{d}v} = \frac{1}{U^2\cos^2\phi}U\cos\phi(-\cos\alpha)$$

and hence

$$\left.\frac{\mathrm{d}\phi_R}{\mathrm{d}v}\right|_{v=0} = \frac{-\cos\alpha\cos\phi}{U}. \tag{A.6}$$

Similarly, differentiating Eq. (2) with respect to v, and noting Eq. (3), yields

$$\left.\frac{\mathrm{d}\alpha_R}{\mathrm{d}v}\right|_{v=0} = \frac{\sin\alpha}{U\sin\phi}. \tag{A.7}$$

Considering the remaining derivatives in Eq (A.1), for vibrations in a given plane, α is constant, and so

$$\frac{\mathrm{d}}{\mathrm{d}v}(\cos(\alpha+\alpha_D)) = \cos\alpha\frac{\mathrm{d}(\cos\alpha_D)}{\mathrm{d}v} - \sin\alpha\frac{\mathrm{d}(\sin\alpha_D)}{\mathrm{d}v} \tag{A.8}$$

and

$$\frac{\mathrm{d}}{\mathrm{d}v}(\sin(\alpha+\alpha_D)) = \sin\alpha\frac{\mathrm{d}(\cos\alpha_D)}{\mathrm{d}v} + \cos\alpha\frac{\mathrm{d}(\sin\alpha_D)}{\mathrm{d}v}, \tag{A.9}$$

where, considering Fig. 2,

$$\frac{\mathrm{d}(\cos\alpha_D)}{\mathrm{d}v} = \frac{\mathrm{d}}{\mathrm{d}v}\left(\frac{U\sin\phi - v\cos\alpha}{U_{NR}}\right) = \frac{1}{U_{NR}^2}\left[U_{NR}(-\cos\alpha) - (U\sin\phi - v\cos\alpha)\frac{\mathrm{d}U_{NR}}{\mathrm{d}v}\right], \tag{A.10}$$

where U_{NR} is the component of the relative velocity normal to the cylinder axis (Fig. 2b), given by

$$U_{NR} = \sqrt{U^2\sin^2\phi - 2Uv\sin\phi\cos\alpha + v^2}, \tag{A.11}$$

and hence

$$\left.\frac{\mathrm{d}U_{NR}}{\mathrm{d}v}\right|_{v=0} = -\cos\,\alpha. \tag{A.12}$$

Similarly to Eq. (A.10),

$$\frac{\mathrm{d}(\sin\,\alpha_D)}{\mathrm{d}v} = \frac{1}{U_{NR}^2}\left(U_{NR}\sin\,\alpha - v\sin\,\alpha\frac{\mathrm{d}U_{NR}}{\mathrm{d}v}\right). \tag{A.13}$$

Finally, Eqs. (A.2)–(A.13) are substituted into Eq. (A.1), which is rearranged to give the general expression

$$\begin{aligned}\zeta_a = \frac{\mu\,\mathrm{Re}}{4m\omega_n}\cos\,\alpha\Bigg\{&\cos\,\alpha\left[C_D\left(2\sin\,\phi + \frac{\tan^2\alpha}{\sin\,\phi}\right) + \frac{\partial C_D}{\partial\,\mathrm{Re}}\mathrm{Re}\sin\,\phi + \frac{\partial C_D}{\partial\phi}\cos\,\phi - \frac{\partial C_D}{\partial\alpha}\frac{\tan\,\alpha}{\sin\,\phi}\right]\\ &-\sin\,\alpha\left[C_L\left(2\sin\,\phi - \frac{1}{\sin\,\phi}\right) + \frac{\partial C_L}{\partial\,\mathrm{Re}}\mathrm{Re}\sin\,\phi + \frac{\partial C_L}{\partial\phi}\cos\,\phi - \frac{\partial C_L}{\partial\alpha}\frac{\tan\,\alpha}{\sin\,\phi}\right]\Bigg\}.\end{aligned} \tag{A.14}$$

References

Bursnall, W.J., Loftin, L.K., 1951. Experimental investigation of the pressure distribution about a yawed circular cylinder in the critical Reynolds number range. US National Advisory Committee for Aerodynamics, Technical Note 2463.

Caetano, E.S., Cunha, A.F., 2003. Identification of parametric excitation at the International Guadiana Bridge. In: Proceedings of fifth International Symposium on Cable Dynamics. Santa Margherita Ligure, Italy, pp. 525–532.

Carassale, L., Freda, A., Piccardo, G., 2004. Quasi-static model for aerodynamic instability of yawed circular cylinders. In: Proceedings of fifth International Colloquium on Bluff Body Aerodynamics and Applications, Ottawa, Canada, pp. 401–404.

Cheng, S., Larose, G.L., Savage, M.G., Tanaka, H., 2003a. Aerodynamic behaviour of an inclined circular cylinder. Wind & Structures 6, 197–208.

Cheng, S., Irwin, P.A., Jakobsen, J.B., Lankin, J., Larose, G.L., Savage, M.G., Tanaka, H., Zurell, C., 2003b. Divergent motion of cables exposed to skewed wind. In: Proceedings of fifth International Symposium on Cable Dynamics. Santa Margherita Ligure, Italy, pp. 271–278.

Davenport, A.G., 1962. Buffeting of a suspension bridge by storm winds. Journal of the ASCE Structural Division 88 (ST3), 233–264.

Davis, D.A., Richards, D.J.W., Scriven, R.A., 1963. Investigation of conductor oscillation on the 275 kV crossing over the Rivers Severn and Wye. Proceedings IEE 110 (1), 205–219.

Den Hartog, J.P., 1956. Mechanical Vibrations, fourth ed. McGraw-Hill, New York.

ESDU, 1986. Mean forces, pressures and flow field velocities for circular cylindrical structures: single cylinder with two-dimensional flow. Engineering Sciences Data Unit International, Item 80025, Amendment C.

Langsoe, H.E., Larsen, O.D., 1987. Generating mechanisms for cable stay oscillations at the Faro Bridges. In: Proceedings of International Conference on Cable-stayed Bridges, Bangkok, Thailand, pp. 1023–1033.

Larose, G.L., Zan, S.J., 2001. The aerodynamic forces on stay cables of cable-stayed bridges in the critical Reynolds number range. In: Proceedings of 4th International Symposium on Cable Dynamics. Montreal, Canada, pp. 77–84.

Larose, G.L., Savage, M.G., Jakobsen, J.B., 2003. Wind tunnel experiments on an inclined and yawed circular cylinder in the critical Reynolds number range. In: Proceedings of 11th International Conference on Wind Engineering, Lubbock, Texas, USA, pp. 1705–1712.

Lowson, M.V., Ponton, A.J.C., 1991. Symmetric and asymmetric vortex flows at high angle of attack, AIAA-91-0276. In: Proceedings of 29th Aerospace Sciences Meeting, Reno, Nevada, USA.

Macdonald, J.H.G., 2002. Separation of the contributions of aerodynamic and structural damping in vibrations of inclined cables. Journal of Wind Engineering & Industrial Aerodynamics 90, 19–39.

Martin, W.W., Currie, I.G., Naudascher, E., 1981. Streamwise oscillations of cylinders. ASCE Journal of Engineering Mechanics 107 (EM3), 589–607.

Matsumoto, M., 1998. Observed behavior of prototype cable vibration and its generation mechanism. In: Proceedings of International Symposium. Advances in Bridge Aerodynamics, Copenhagen, Denmark, pp. 189–211.

Matsumoto, M., Hikami, Y., Kitazwa, M., 1994. Cable vibration and its aerodynamic/mechanical control. In: Proceedings of Internal Conference on Cable-stayed and Suspension Bridges, Deauville, France, vol. 2, pp. 439–452.

Melby, S., Hovland, K., Østlid, H., 1994. Construction and maintenance of two-cable-stayed bridges in adverse environment. In: Proceedings of 3rd Symposium on Straits Crossings, Ålesund, Norway, Balkema, Rotterdam.

Owen, J.S., 2002. Drag instability and the response of lighting columns to wind loading. In: Proceedings of 5th UK Conference on Wind Engineering, Nottingham, UK.

Saito, T., Matsumoto, M., Kitazawa, M., 1994. Rain-wind excitation of cables on cable-stayed Higashi-Kobe Bridge and cable vibration control. In: Proceedings of International Conference on Cable-stayed and Suspension Bridges, Deauville, France, vol. 2, pp. 507–514.

Schewe, G., 1983. On the force fluctuations acting on a circular cylinder in crossflow from subcritical up to transcritical Reynolds numbers. Journal of Fluid Mechanics 133, 265–285.

Smith, B.W., Wyatt, T.A., 2003. Structures, Dynamics and Wind—a 10-year review, eighth Biennial Scruton Lecture, UK Wind Engineering Society.

Svensson, B., Emanuelsson, L., Svensson, E., 2004. Øresund Bridge—Cable system—Vibration incidents, mechanisms and alleviating measures. In: Proceedings of 4th International Cable Supported Bridge Operators' Conference, Copenhagen, Denmark, pp. 99–108.

Thomson, K.D., Morrison, D.F., 1971. The spacing, position and strength of vortices in the wake of slender cylindrical bodies at large incidence. Journal of Fluid Mechanics 50, 751–783.

Van Dyke, P., Laneville, A., 2004. Galloping of a single conductor covered with a D-section on a high voltage overhead test line. In: Proceedings of fifth International Colloquium Bluff Body Aerodynamics and Applications, Ottawa, Canada, pp. 377–380.

Virlogeux, M., 1998. Cable vibrations in cable-stayed bridges. In: Proceedings of International Symposium on Advances in Bridge Aerodynamics, Copenhagen, Denmark, pp. 213–233.